Synthesis of nano-structured stainless steel powder by mechanical alloying-an overview

R. Shashanka
Department of Chemistry, School of Engineering, Presidency University, Bengaluru-560064, India.
Corresponding author:
E-mail: shashankaic@gmail.com

Abstract— The synthesis of different types of nano-structured stainless steel powders from elemental Fe, Ni, Cr powder with alloying elements by mechanical alloying is reviewed. A fundamental study shows the possibility of formation of nano-structured stainless from elemental metals by mechanical alloying. There is a tendency of decreasing their grain sizes to nano range after mechanical alloying and reaches constant after several hours of milling. The progress of milling, continuous amorphization, structural and phase evolution of stainless steel have been reviewed by means of X-ray diffraction, scanning and transmission electron microscopy, thermo-gravimetric and differential scanning calorimetric analysis. The mechanical properties of the sintered stainless steels are also presented.

Index Terms— Ball mill, mechanical alloying, nano-structure, powder metallurgy, stainless steel

1 INTRODUCTION

Stainless steel is the generic name for a number of different steels used primarily for their resistance to corrosion. The one key element they all share is a certain minimum percentage (by mass) of chromium: 10.5%. Although other elements, particularly nickel and molybdenum, are added to improve corrosion resistance, chromium is always the deciding factor. All stainless steels are iron-based alloys that contain a minimum of around 10.5% Chromium. The Chromium in the alloy forms a self-healing protective clear oxide layer. This oxide layer gives stainless steel their corrosion resistance [1]. The self-healing nature of the oxide layer means the corrosion resistance remains intact regardless of fabrication methods. Even if the material surface is cut or damaged, it will self-heal and corrosion resistance will be maintained [1]. Even trace amounts of some elements can markedly alter the corrosion resistance. Grades high in Chromium, molybdenum and nickel are the most resistant to corrosion. About 10% chromium is used to fabricate low carbon steel which is extremely resistant to heat, corrosion and all kinds of impact making it a better alternative to carbon steel [2]. Carbon steel when exposed to moist air can be susceptible to rusting. Advantages of stainless steel include corrosion resistant, high tensile strength, good weldability, high temperature oxidation resistant, fire and heat resistant [3-5]. Stainless steel products are also used in hospitals, food processing plants, kitchens as they can be easy to clean [6-8]. This makes it a more hygienic option. Shiny and lustrous surface of steel also gives it an attractive appearance making it favorite for kitchen and home equipments. Stainless steel also requires less maintenance and happens to be long lasting. Moreover it can be cut, melded, welded, reshaped and fabricated with greater ease than carbon steel. Stainless steel fabrication is therefore much easier and popular [9, 10]. Mechanical alloying is one of the important and popular methods to fabricate nano-structured stainless steel powders [11-13]. The researchers are trying to prepare nano-structured stainless steels powders due to its wide range of applications as well as unusual behavior of all the materials in its nano size [14, 15].

1.1. DIFFERENT TYPES OF STAINLESS STEEL AND THEIR PROPERTIES

The original form of stainless steel, (iron with around 12% Chromium) is still in widespread use, and engineers now have a wide choice of different types (grades). In all, there are more than 100 different grades but these are usually sub-classified into distinct metallurgical "families" such as the *austenitic, ferritic, martensitic and duplex* families [16, 17]. The proportions of iron to chromium may be varied and other elements such as nickel, molybdenum, manganese and nitrogen may be added to widen the range of capabilities [3, 7]. Each particular grade of stainless steel has its own unique mechanical and physical properties and will usually be produced in accordance with an established national or international specification or standard.

A Schaeffler diagram can be used to represent the effect of proportion of two elements (and therefore the composition of the alloy) on the structure obtained after cooling from 1050° C to room temperature [8].

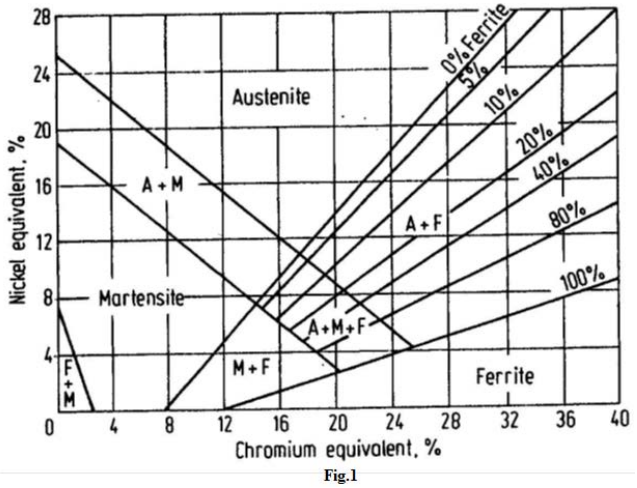

Fig.1

Fig. 1 shows Schaeffler – de Long diagram [18]

Fig. 1 shows Schaeffler – de Long diagram. It shows the limits of the austenitic, ferritic and martensitic phases in relation to the chromium and nickel equivalent, calculated by using these expressions [18].

Cr equivalent = % Cr + 1.0 (% Mo) + 0.5 (% Nb + % Ta) + 1.5 (% Si) + 2 (% Ti) + (% W + % V + % Al)

Ni equivalent = % Ni + 30 (% C) + 0.5 (% Mn) + 30 (% N) + 0.5 (%Co)

The high chromium content of stainless steel also helps to resist scaling at elevated temperatures. The elongation for austenitic stainless steel is quite high [7]. High ductility and high work hardening rates allows austenitic stainless steel to be formed using severe processes such as deep drawing. At cryogenic temperatures the tensile strengths of austenitic stainless steel are also substantially higher than at ambient temperatures [19]. They also maintain excellent toughness [4]. However, ferritic, martensitic and precipitation hardening stainless steels should not be used at sub-zero temperatures. The toughness of these grades drops significantly at low temperatures. The duplex stainless steel has higher tensile strengths than austenitic steels [19]. Table 1 shows some of the properties of different types of stainless steel [20, 21].

Table 1 [20, 21]

Types of Stainless steel	Density (g/cm^3)	Young's modulus (N/mm^2) Or (MPa)	Thermal expansion ($X10^{-6}/^{\circ}c$) 200-600°c	Thermal conductivity ($w/m^{\circ}c$) 20°c	Heat capacity ($J/Kg^{\circ}c$) 20°c	Tensile strength (ksi)	Yield strength (ksi)	Rockwell hardness
Martensitic*	7.6-7.7	220,000	12-13	22-24	460	180 (heat treated)	150 (heat treated)	C34
Ferritic	7.6-7.8	220,000	12-13	20-23	460	70-75	40-45	B65-75
Austenitic	7.9-8.2	195,000	17-19	12-15	440	85-150	40 min	B85-95
Duplex	8	200,000	13	20	400	116	80	------

* in the hardened and tempered condition

1.2. MECHANICAL ALLOYING

Mechanical alloying is the modern and very popular method to synthesis nanostructured stainless steel powder [22, 9, 10]. Nanostructured stainless steel have been synthesized by a number of techniques starting from the surface nano crystallization of stainless steel induced by ultrasonic shot peening [23], hydraulic pressings [24] and synthesis of ultrafine grained 304 stainless steel through machining [25]. But the advantage of using MA for the synthesis of nanocrystalline materials lies in its ability to produce bulk quantities of material in the solid state using simple equipment and at room temperature [2]. Additionally, a mechanically alloyed powder reduces oxidation of the constituent powders, related to the shortened time of processing [26]. The effect of particle size of iron powder on α to γ transformation in the nanostructured high nitrogen Fe–18Cr–10Mn–4Mo stainless steel, produced by mechanical alloying (MA) was investigated by Tehrani et al. [27].

Mechanical alloying (MA) is a powder processing technique that allows production of homogeneous materials starting from blended elemental powder mixtures. A number of investigations have been carried out at the beginning from the mid-1980s to synthesize a variety of stable and metastable phases including supersaturated solid solutions, crystalline and quasicrystalline intermediate phases, and amorphous alloys [28]. The actual process of MA starts with mixing of the powders in the right proportion and loading the powder mix into the mill along with the grinding medium (generally steel balls). This mix is then milled for the desired length of time until a steady state is reached when the composition of every powder particle is the same as the proportion of the elements in the starting powder mix. The milled powder is then consolidated into a bulk shape and heat treated to obtain the desired microstructure and properties. Some of the experimental studies on synthesis of stainless steel by mechanical alloying are also shown in **Table 2.**

Table 2

Type of Stainless steel	Composition	Type of mill	Experimental conditions	Year	Main findings	Reference
Duplex	Fe-18Cr-8Ni	Planetary ball mill	13h, Ar atmosphere, 235 rpm, BPR is 6:1, Annealed at 700°C, air cooled	2007	Heat treatment of as milled powders resulted in dual phase	[29]
Austenite	Fe-18Cr-11Mn	High energy ball mill	100h, N_2 atmosphere, 300 rpm, BPR is 25:1	2008	Nitrogen favors the austenitic phase transformation	[30]
Duplex	Fe-18Cr-13Ni	Dual drive planetary mill	10h, Toluene atmosphere, BPR is 6:1, 12:1, stearic acid	2015	Addition of stearic acid and increase in BPR decreases the grain size and favors the γ-phase formation	[3]
Duplex	Fe-18Cr-13Ni	Dual drive planetary mill	10h, Toluene atmosphere, BPR is 6:1	2015	Formation of dual phase (Austenite and ferrite)	[7]

2. Characterization of Stainless Steel

2.1. XRD analysis

XRD analysis of different stainless steel powder is reviewed successfully. XRD patterns of the Fe –18Cr –12Mn – xN (x is the nitrogen concentration in wt. %) powder milled in a high-energy shaker mill for 120 h and then sintered at 1200°C for 2 h. Reducing the Mn content increases the chemical potential for austenite stability and reduces the α to γ transformation rate [31]. It is observed that to obtain an austenitic structure, the samples were immediately water-quenched after sintering. The analysis of the XRD results suggests that fully austenitic structures have been obtained after the densification process by E. Salahinejad et al. [32]. It is of interest to study the structural transitions occurring during annealing.

Fig. 2 shows the XRD patterns of austenitic and ferritic stainless steel powders milled in planetary mill for 30 h. The spectra shows the presence of diffraction peaks of ferrite (α) after milling whereas after air-cooling and furnace cooling both austenite (γ) and martensite (α) peaks are present. A comparison of intensity ratio of α and γ peaks suggests that air-cooled sample contains a higher fraction of retained austenite than furnace-cooled sample. During annealing at 700°C the metastable α phase is converted to the stable γ phase is investigated by M.H. Enayati et al. [33]. It has been widely accepted that during MA, the enthalpy of the components increases due to defects introduction and increased internal energy [34, 12].

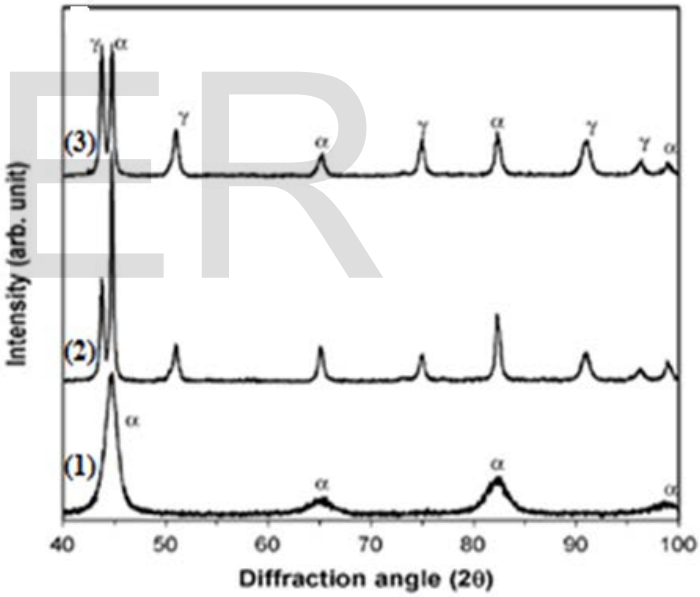

Fig. 2 XRD spectra of Fe–18Cr–8Ni alloy as-milled and after subsequent heat treatment at 700°C for 1 h; (1) as-milled (2) furnace-cooled and (3) air-cooled samples [33]

This could act as the driving force for solid-state amorphization and phase transformation during MA [35]. The XRD analysis of the milled powders of the composition 80.68Fe-15.34Cr-2.98W-0.5Y-0.25Ti-0.26V and detailed characterization studies of the synthesized steel powders and the subsequent optimization of the milling parameters have been reported elsewhere [36, 37].

2.2. Scanning Electron Microscopy

During the mechanical milling process, the powder particles are repeatedly flattened, cold welded, fractured and rewelded [28, 13]. **Fig. 3 (a, b, c, d, e)** shows the SEM micrograph of the Fe-18Cr-12Mn powder milled in a planetary ball mill for various time periods. The irregular nature of the powder particles is obvious in the low milling times; however, in the higher milling times the particles have a higher uniformity and the shape of the particles becomes rounded.

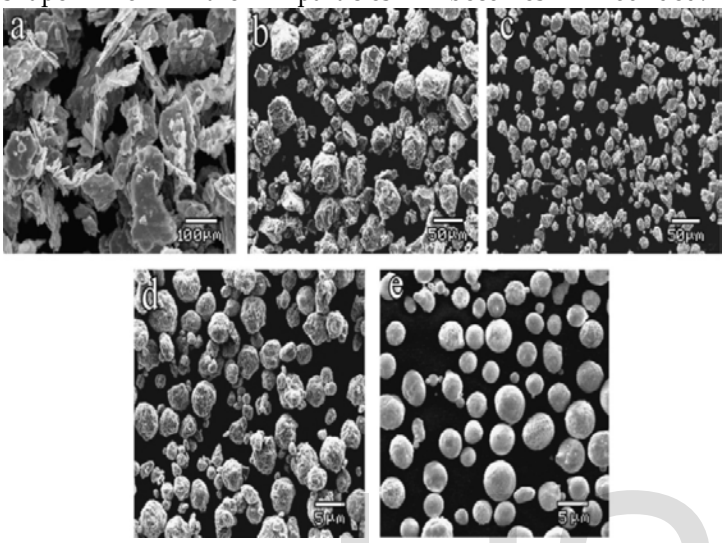

Fig. 3 Morphological changes of the Fe-18Cr-12Mn milled powders as a function of the milling time **(a)** 6 h; **(b)** 24 h; **(c)** 48 h; **(d)** 96 h; **(e)** 144 h [38]

At the initial stages of the ball milling process (e.g. 6 h), due to the ball-powder-ball collisions, the high level of compressive forces were introduced into the powder particles and the particles obtained from this stage are the large agglomerated composite particles with a flattened morphology as shown in as evident from **Fig. 3 (a)** by R. Amini et al. [38].

The development of the MA process leads to a drastic fragmentation of the agglomerated particles and consequently the production of smaller particles with irregular shapes and a wide size distribution, as presented in **Fig. 3 (b).** This phenomenon is attributed to the severe shear and impact forces applied to the powder particles during the high-energy ball milling process. After the sufficient milling time, the powder particles tend to reduce in size and show an irregular shape with a narrow size distribution as clear from **Fig. 3 (c).** By further progression of the MA process, the homogeneity of the powders increases and the powder particles become regular in shape as shown in **Fig. 3 (d).** Finally, the powder of the end-product (144 h) comprises homogeneous and smooth spheres with an average size of about 4μm in diameter, as presented in **Fig. 3 (e).** The last stage of the MA process in which all the particles are uniform in shape and in size signifies the completion of the solid state amorphization reaction [38, 39].

2.3. Thermal analysis

Thermal analysis consists of a family of analytical techniques in which a property of the sample is monitored against time or temperature while the temperature of the sample is programmed. The properties include weight, dimension, energy take up, differential temperature, dielectric constant, and other less common attributes [7]. **Fig. 4** depicts the results of the DSC analysis of Fe–18Cr–8Mn powder mixture milled under a continuous flow of high-purity nitrogen gas and under an argon atmosphere for 168 h. It is noticeable that the DSC scans reveal exothermic events well in the same temperature ranges [7]. Previous studies have implied that the first peak corresponds to the transformation of the γ-phase to α-phase and the second one is related to crystallization of the amorphous phase [40, 41]. As these transformations are not essentially accompanied by any weight loss, both the weight losses are attributed to nitrogen atoms leaving the structure during heating. Indeed, these weight losses are owing to the lower nitrogen Solubility of the products compared to the parent phases [29].

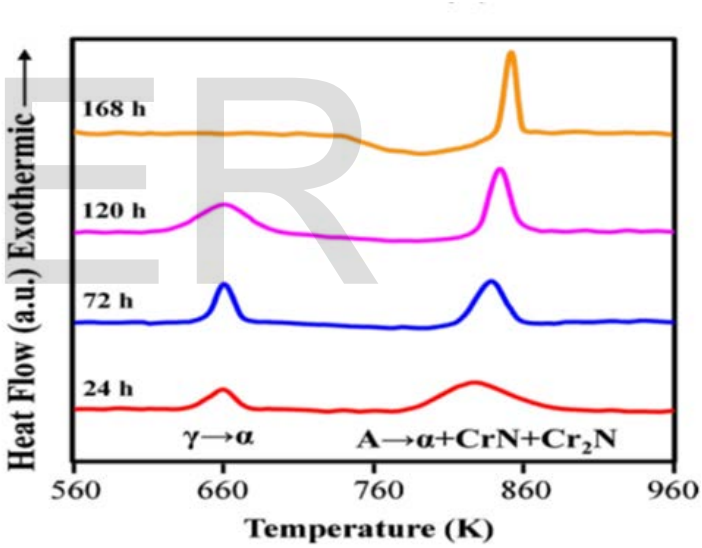

Fig. 4 DSC graph of Fe–18Cr–8Mn powder milled under nitrogen [40, 41, 29]

2.4. Transmission Electron Microscopy

The elemental powder of 78Fe–18Cr–4Mn (wt.%) composition was milled in a planetary ball mill (Fritsch, Pulverisette 5) in a sealed container with a capacity of 250 ml that had been filled with pure nitrogen gas. A rotation speed of 250 rpm and a ball to powder weight ratio of 30:1 was maintained [42]. TEM micrograph of above milled powder for 117 and 126 h having the nanocomposite and amorphous structures respectively, in accordance with the XRD analyses by E. Salahinejad et al. [42]. The selected area diffraction (SAD) patterns related to the sample milled for 117 h imply that the dark regions are a combination of the nanocrystalline α and γ-phases and the bright

matrix is a featureless amorphous phase **(Fig. 5a).** On the contrary, the TEM micrograph of the sample milled for 126 h exhibits no contrast and the corresponding SAD pattern represents a homogenous hallo pattern attributed to a fully amorphous structure **(Fig. 5b)**. No diffraction spots or sharp diffraction rings related to crystalline phases can be detectable and merely diffraction hallos associated with the amorphous phase can be observed. Thus, two major microstructural evolutions were detected during MA of the powder: nanograin refinement and amorphization. The TEM powder samples were prepared by dispersing the powder particles in ethanol and dropping down them in a copper rigid.

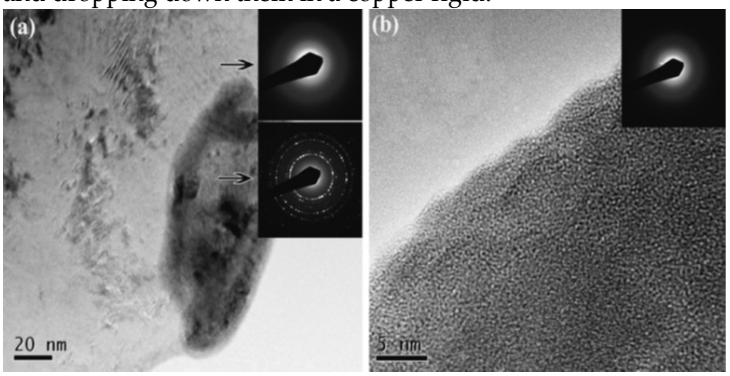

Fig. 5 TEM micrograph of 78Fe–18Cr–4Mn powders milled for (a) 117 and (b) 126 h. The insets indicate the SAD pattern of the different regions [42]

3. Sintering of stainless steel powder

The first step of powder densification is usually accomplished by pressing powder particles to create some initial contacts among them [5]. This process should be accompanied by particle rearrangement and plastic compaction [7]. In spite of applying a considerable compressive pressure up to 800 MPa, a relative density of as small as 69% was obtained for the powdered Fe–18Cr–8Mn–0.973N stainless steel particles milled under a nitrogen gas atmosphere for 48 h and maintaining the powder standard weight ratio of 75:25 by E. Salahinejad et al. [43]. It is well known that the efficiency of compaction is heavily dependent on the morphology and hardness of powder particles. The irregular morphology and high hardness of powders contribute to low green densities. In fact, poor packing behavior of powders with irregular morphologies causes a broad pore size distribution that can inhibit sintering progress. If the powder particles are near-spherical in shape, then the relatively low green density is attributed to the severe plastic deformation subjected to the particles during milling, which has promoted a high level of strain hardening. This suppresses more plastic deformation during the cold compaction step, leading to the relatively ineffective compact ability. Austenitic stainless steels are found to undergo sintering by lattice (volume) diffusion in the intermediate stage and by a combination of grain boundary and lattice diffusion in the final stage [30].

The thermal stability of the amorphous phase was assessed in a differential scanning calorimeter under a flowing argon gas atmosphere [44]. Here, the effect of the amorphous phase presence on the densification kinetics is noticeable. Since the solubility of nitrogen is limited in the crystalline structures, nitrogen atoms tend to accumulate in the amorphous phase to decrease strain energy. The introduced nitrogen atoms occupy the interstitial sites of the atomic polyhedra or clusters of the amorphous structure, contributing to an increase in the dense random packing. This decreases the atomic diffusion coefficients, retarding densification accomplished by diffusion. On the other hand, due to the high affinity of Fe, Cr, and Mn for nitrogen and also the strong attractive bonds made up between the metal-nitrogen pairs, the N atoms do not tend to be neighbors to each other. Subsequently, the N atoms are surrounded by the metallic atoms. The presence of these stiff metal-nitrogen atomic pairs decreases the atomic mobility which is required for diffusion. Also, as the amorphous phase is the continuous phase in the microstructure, there is no rapid diffusion path like grain boundary in the structure. The contribution of these factors is responsible for slow atomic diffusivities and consequently the slow densification rate.

4. Mechanical properties studies

The metallic elements of 74Fe–18Cr–8Mn (wt. %) composition was mechanically milled in a high-energy shaker mill, and milling was conducted under a continuous flow of pure nitrogen gas for durations of 48, 72, 96, and 120 h. The as-milled powders were uniaxially cold-pressed to cylinders at a compressive pressure of 1 GPa [45]. To prevent oxidation during sintering and to preserve nitrogen in the structure, the compacts were encapsulated in quartz tubes under an evacuated condition (10^{-5} atm). The densification was performed by sintering at 1100°C for 20 h and subsequently water quenching to room temperature to achieve an austenitic structure. It is seen that the microhardness of the sintered material, which is not affected by pores in contrast to the bulk hardness and yield stress, is considerable values. It is due to the fine structure and high-nitrogen content of the materials. It is well established that nanostructured materials exhibit higher hardnesses and strengths compared to coarse-grained materials, as expected from the Hall–Petch equation [45]. Moreover, it has been found that the nitrogen addition to austenitic stainless steels enhances their hardness and strengths.

It has been reported that micron-grained Fe–23Cr–2Mo–1N and Fe–25Cr–1N austenitic stainless steels having 45% Lotus-type pores show the compressive strengths of 270 and 290MPa with pores aligned parallel to the compression direction and those of 90 and 180MPa with pores aligned perpendicular to the compression direction, respectively [46]. Obviously, the yield strength and bulk hardness of porous materials depend

not only on those of matrix but also on the porosity. There are several empirical equations and theoretical models predicting the room temperature strength of austenitic stainless steels. A number of them correlate the yield stress with the chemical composition and grain size of stainless steels, including for nickel-free austenitic stainless steels [47].

5. Conclusion

The MA process for different types of stainless steel with nominal composition is reviewed and it is a very simple and easy technique to prepare stainless steels. Different types of stainless steels can be prepared through mechanical alloying while optimizing different milling conditions and proper composition of starting materials. These stainless steels differ to one another in thermal, mechanical and magnetic properties. As the milling time increases there will be decrease in grain size of the stainless steel and further milling resulted in a significant decrease in the major peak intensity and increases it's broadening due to the grain refinement, introduction of lattice strain and development of the amorphous phase. The improvement in mechanical properties of stainless steel with milling has also been improvement.

References

[1] British Stainless Steel Association, SSAS Information Sheet No.1.1, Issue 02, pp. 1-3, 12th March 2001.

[2] R. Shashanka, D. Chaira, Powder Technol. vol. 259, pp. 125–136, 2014.

[3] R. Shashanka, D. Chaira, Powder Technol. vol. 278, pp. 35-45, 2015.

[4] R. Shashanka, D. Chaira, B.E. Kumara Swamy, Int. J. Electrochem. Sci. vol. 10, pp. 5586–5598, 2015.

[5] R. Shashanka, D. Chaira, Acta Metall. Sin. (Engl. Lett.). vol. 29, pp. 58-71, 2016.

[6] Mohan, V. Hygenic importance of stainless steel in developing countries, **I**nternational **Stainless S**teel **F**orum, downloadable from www.worldstainless.org.

[7] R. Shashanka, D. Chaira, Mater Charact. vol. 99, pp. 220-229, 2015.

[8] R. Shashanka. D. Chaira, D. Chakravarty, Journal of Materials Science and Engineering B, vol. 6 (5-6), pp. 111-125, 2016.

[9] R. Shashanka, D. Chaira, B.E. Kumara Swamy, International Journal of Scientific & Engineering Research. vol. 6, pp. 1863–1871, 2015.

[10] R. Shashanka, D. Chaira, B.E. Kumara Swamy, International Journal of Scientific & Engineering Research, vol. 7, pp. 1275-1285, 2016.

[11] R. Shashanka. D. Chaira, Tribology Transactions. vol. 60, pp. 324-336, 2017.

[12] Shalabh Gupta, R. Shashanka, D. Chaira, IOP Conf. Series: Materials Science and Engineering. vol. 75, pp. 012033, 2015.

[13] A.K. Nayak, R. Shashanka, D. Chaira, IOP Conf. Series: Materials Science and Engineering, vol. 115, pp. 012008, 2016.

[14] Shashanka Rajendrachari, Bahaddureghatta E. Kumara Swamy, Sathish Reddy, Debasis Chaira, Anal. Bioanal. Electrochem. vol. 5, pp. 455–466, 2013.

[15] Sathish Reddy, B. E. Kumara Swamy, S. Aruna, Mohan Kumar, R. Shashanka, H. Jayadevappa, Chemical Sensors, vol. 2, pp. 1-7, 2012.

[16] Salahinejad, E. Amini, R. Hadianfard, M.J. Powder Technology. vol. 215(216), pp. 247–253, 2012.

[17] Guide to Stainless Steel Finishes (Building Series, Volume 1), Luxembourg: Euro Inox, 2005.

[18] Schaffeler diagram, Ir G HENDERIECKX, GIETECH BV, March, 2006.

[19] Stainless Steels - Introduction to grades, properties and applications, Supplier Data by Aalco.

[20] Béla Leffler, stainless steels and their properties, www.outokumpu.com.

[21] Practical guidelines for the fabrication of Duplex stainless steel, International Molybdenum Association (IMOA), London, UK, 2009

[22] R. Shashanka. D. Chaira, Transactions of PMAI. vol. 41, pp. 17-25, 2015.

[23] Liu, G. Lu, J. Lu, K. Materials Science and Engineering A. vol. 286, pp. 91–95, 2000.

[24] Dobrzañski, L.A. Brytan, Z. Actis Grande, M. Rosso, M. Archives of Materials Science and Engineering, vol. 28, pp. 217-223, 2007.

[25] Senthilkumar, V. Lenin, K. Journal of Minerals & Materials Characterization & Engineering. vol. 10, pp. 455-461, 2011.

[26] R. Shashanka, Fabrication of Nano-Structured Duplex and Ferritic Stainless Steel by Planetary Milling Followed by Consolidation, PhD thesis, 2016.

[27] Tehrani, F. Abbasi, M.H. Golozar, M.A. Panjepour, M. Materials Science and Engineering A. vol. 528, pp. 3961–3966, 2011.

[28] Suryanarayana, C. Prog. Mater. Sci. vol. 46, pp. 1–184, 2001.

[29] Amini, R. Salahinejad, E. Hadianfard, M.J. Askari Bajestani, E. Sharifzadeh, M. J. Alloys Compd. vol. 509, pp. 2248–2251, 2011.

[30] Suri, P. Koseski, R.P. German, R.M. Mater Sci Eng A. vol. 402, pp. 341–8, 2005.

[31] Tehrani, F. Golozar, M.A. Abbasi, M.H. Panjepour, M. Materials Science and Engineering A. vol. 534, pp. 203– 208, 2012.

[32] Salahinejad, E. Amini, R. Hadianfard, M.J. Materials and Design. vol. 31, pp. 2241–2244, 2010.

[33] Enayati, M.H. Bafandeh, M.R. Nosohian, S. J. Mater. Sci. vol. 42, pp. 2844–2848, 2007.

[34] De Lima, J.C. Dos Santos, V.H.F. Phys. Rev. B, vol. 62 (13), pp. 8871–8877, 2000.

[35] Haghir, T. Abbasi, M.H. Golozar, M.A. Panjepour, M. Materials Science and Engineering A. vol. 507, pp. 144–148, 2009.

[36] Kavithaa, S. Subramanian, R. Angelo, P.C. Shankar, P. Nat J Technol. vol. 5, pp. 81, 2009.

[37] Kavithaa, S. Subramanian, R. Angelo, P.C. Trans Indian Inst Met. vol. 63, pp. 67, 2010.

[38] Amini, R. Shokrollahi, H. Salahinejad, E. Hadianfard, M.J. Marasi, M. Sritharan, T. Journal of Alloys and Compounds. vol. 480, pp. 617–624, 2009.

[39] Sherif El-Eskandarany, M. Bahgat, A.A. Gomaa, N.S. Eissa, N.A. J. Alloys Compd. vol. 290, pp. 181–190, 1999.

[40] Amini, R. Salahinejad, E. Hadianfard, M.J. Marasi, M. Sritharan, T. Materials Science and Engineering A. vol. 527, pp. 1135–1142, 2010.

[41] Amini, R. Hadianfard, M.J. Salahinejad, E. Marasi, M. Sritharan, T. J. Mater. Sci. vol. 44, pp. 136–148, 2009.

[42] Salahinejad, E. Amini, R. Askari Bajestani, E. Hadianfard, M.J. J. Alloys Compd. vol. 497, pp. 369–372, 2010.

[43] Erfan Salahinejad, Rasool Amini, Mehdi Marasi, Mohammad Jafar Hadianfard, Materials and Design. vol. 31, pp. 527–532, 2010.

[44] Amini, R. Hadianfard, M.J. Salahinejad, E. Marasi, M. Sritharan, T. J Mater Sci. vol. 44, pp. 136–148, 2009.

[45] Salahinejad, E. Amini, R. Hadianfard, M.J. Materials Science and Engineering A. vol. 527, pp. 5522–5527, 2010.

[46] Alvarez, K. Sato, K. Hyun, S.K. Nakajima, H. Mater. Sci. Eng. C. vol. 28, pp. 44–50, 2008.

[47] Balachandran, G. Bhatia, M.L. Ballal, N.B. Rao, P.K. ISIJ Int. vol. 41, pp. 1018–1027, 2001.